How newly developed shale gas facilities influence soil erosion in a karst region in SW China

Yu Guo, Xianyuan Du, Dandan Li, Guodi Zheng, Xinyu Zhang, Hongkun Chen, Jin Zheng

PII: S0048-9697(21)06901-1

DOI: https://doi.org/10.1016/j.scitotenv.2021.151825

Reference: STOTEN 151825

To appear in: *Science of the Total Environment*

Received date: 31 July 2021

Revised date: 26 October 2021

Accepted date: 16 November 2021

Please cite this article as: Y. Guo, X. Du, D. Li, et al., How newly developed shale gas facilities influence soil erosion in a karst region in SW China, *Science of the Total Environment* (2021), https://doi.org/10.1016/j.scitotenv.2021.151825

How newly developed shale gas facilities influence soil erosion in a karst region in SW China

Yu Guo[1], Xianyuan Du[2], Dandan Li[1,2], Guodi Zheng[3,4,*], Xinyu Zhang[1,4], Hongkun Chen[2], Jin Zheng[2]

[1]Key Laboratory of Ecosystem Network Observation and Modeling, Institute of Geographic Sciences and Natural Resources Research, Chinese Academy of Sciences, Beijing 100101, China

[2]State Key Laboratory of Petroleum Pollution Control, CNPC Research Institute of Safety and Environment Technology, Beijing 102206, China

[3]Center for Environmental Remediation, Institute of Geographic Sciences and Natural Resources Research, Chinese Academy of Sciences, Beijing 100101, China

[4]College of Resources and Environment, University of Chinese Academy of Sciences, Beijing 100190, China

* Corresponding authors

Email addresses: zhengge@igsnrr.ac.cn

Abstract

We already know that the construction of shale gas extraction infrastructure exacerbates soil erosion in vulnerable areas. We are not clear however, about whether the completed well pads and pipelines continue to influence soil erosion after the construction is completed. We applied high-resolution remote sensing images and DEM data from 2014 and 2017 and the Revised Universal Soil Loss Equation (RUSLE) model to calculate how the layout of the well pads and pipelines in a shale gas development area affected soil erosion. We used Geodetector to analyze the factors that affected the soil erosion intensity around the well pads. The results showed that about 0.02% and 0.12% of the total erosion in the shale gas development zone was directly caused by the completed well pads and pipelines in 2014 and 2017, respectively. Most of the erosion was related to the completed pipelines. The completed shale gas well pads affected the soil erosion intensity up to 90 and 60 m from the pads in 2014 and 2017, respectively. The soil erosion around the completed pipelines was mainly from the soil surface over the pipeline and had little effect on the surroundings. The main influences on the soil erosion intensity at different distances from the well pads were land use and slope, and the interactions between them. We suggest that, when developing new shale gas extraction facilities, gas pipelines should be arranged in gently sloping areas, and vegetation should be planted on the bare soil over the pipelines to reduce soil erosion.

Keywords: Well pad, Pipeline, Soil erosion, RUSLE model, Geodetector.

1. Introduction

Soil is disturbed, increasing the risk of soil erosion, when shale gas facilities, including well pads and pipelines, are constructed (Pierre et al., 2015; Chen et al., 2018). At the same time geographical environmental factors and human activities affect the soil erosion process. For example, Drohan and Brittingham (2012) found that there was a higher risk of the soil erosion around a well pad placed on a steep slope is much greater than that around a well pad on a gentle slope in the northern Allegheny Plateau, USA. Approximately 51% (57.9 km^2) of La Salle in the Eagle Ford shale gas development zone is a high risk of soil erosion. Through being disturbed because of changes in land use types, about 2 million tons of soil at a potential risk of erosion every year (Pierre et al., 2015). Mcbroom et al. (2012) reported that the soil erosion rates under natural gas pads with areas of 1.4 and 1.1 ha, at 13,972 and 714 kg ha a^{-1}, respectively, were much higher than the soil erosion rate (111–224 kg ha a^{-1}). Wachal et al. (2009) reported that soil erosion caused by the construction of well pads could be reduced by restoring the vegetation. Shale gas development zones in China are concentrated in the southwestern, geomorphologically diverse, ecologically sensitive, karst area (Zou et al., 2015; Guo et al., 2020; Wang et al., 2018). The rapid development of the shale gas industry and the associated large-scale facilities may cause locally severe soil erosion, and the effects of the developments may endure long after the infrastructure construction is completed. While others have studied soil erosion during the construction phase, there is little information about how completed well pads and pipelines impact on soil

erosion. This study therefore mainly concentrates on how shale gas well pads and pipelines contribute to soil erosion after the construction is completed.

The RUSLE model can be used to calculate soil erosion in shale gas development area. A comparison of the methods used to measure soil erosion in the Eagle Ford shale gas development zone indicated that the RUSLE model was more suitable than the Wind Erodibility Index (WEI) model for areas with severe water erosion and high impacts from human activities (Ma et al., 2018; Pierre et al., 2015; Chen et al., 2017; Zeng et al., 2017). Various analysis methods have been used to measure the drivers of change in soil erosion, including correlation analysis (Jin et al., 2021), analytic hierarchy process, and regression analysis (Xu and Shao, 2006; Yang et al., 2013). We compared these methods and considered that Geodetector, with its high spatial heterogeneity and numerous factors, was the most suitable for quantifying the factors behind the changes in the soil erosion intensity in shale gas development areas (Wang and Xu, 2017). The RUSLE model and Geodetector together provide an effective method for accurately and quantitatively evaluating the influences of completed shale gas well pads and pipelines on soil erosion in karst areas.

In this study, we selected a shale gas development zone in Southwest China as the study area. The objective was to explore the factors that drove soil erosion around completed shale gas infrastructures (e.g., well pads and pipelines) in the karst area. We used the RUSLE model to calculate the distribution of soil erosion intensity in the study area by high-resolution remote sensing interpretation data and DEM data in 2014 and 2017 and the spatial analysis module in ArcGIS was used to analyze the

extent of the impact of well pads and pipelines on the soil erosion intensity. Geodetector was used to determine the main influences on erosion from the well pads. We hypothesized that the soil erosion in the areas around the completed shale gas well pads and pipelines would increase, and that land use and slope would be the strongest influences on soil erosion. The results of this study will provide a robust scientific basis for developing projects to protect water and soil around shale gas industrial sites in karst areas.

2. Materials and methods

2.1 Study area

The study site was a shale gas development area covering 295.28 km^2 (Fig 1A), close to Yibin City in Sichuan Province, South West China. The altitude of the development site ranged from 1148 m in the northeast to 402 m in the west, and the slope was 2°–38°. The topography of the area is dominated by gradual low-relief mountains. As outlined in the 'Ecological Function Zoning of Sichuan Province', the study area belongs to ecological zone I, which represents the subtropical humid climate zone of the Sichuan Basin; ecological subregion I5, which represents karst evergreen broad-leaved forest on the southern margin of the basin, and soil conservation zone I5-1, the Yinan mining industry and soil conservation ecological function zone. The area has an annual average precipitation of 1050–1618 mm, an annual average temperature of 18 °C, and annual average sunshine hours of 1037 hours (CMA Meteorological Data Center, 2018). This is a karst landform area, and the main land use types are forest and dry land. The main types and distribution of soil

are as follows: Calcaric Purpli-Udic Cambosols are mainly distributed in hilly areas, and have mostly been developed as cultivated land. Typic Ferri-Udic Argosols are generally distributed in low, mid-mountain, and hilly areas at altitudes of <1000 m and on river bank terraces. Typic Hapli-Stagnic Anthrosols are mainly distributed on the valley terraces, hills, flat dams, and dissolution trough dams. Carbonati-Perudic Cambosols are mainly distributed in low and middle mountain trough areas where limestone strata are exposed.

In the study area, the shale gas industry has been developed since June 2012. In July 2014, there was a total of 15 well pads and 17 pipelines in the study area, and there were 42 well pads (240 wells) and 39 pipelines in July 2017. The well pads and pipelines are distributed evenly throughout the study area. To support this study, we used high-resolution remote sensing images from 2014 and 2017 and ground surveys (Table S1).

2.2 RUSLE model

The RUSLE model is shown as follows (Renard et al., 1997):

$$A = R \times K \times LS \times C \times P$$

where A is the mean soil loss per unit area (t ha^{-1} a^{-1}); R is the rainfall erosivity factor ha^{-1} a^{-1}, i.e., the erosivity of the rain-runoff (MJ mm ha^{-1} h^{-1} a^{-1}); K is the soil erodibility factor, i.e., the erodibility of the soil (t ha h MJ^{-1} ha^{-1} mm^{-1}); LS is the topographic factor, i.e., the slope length/slope steepness; C is the vegetation cover and management factor, P is the soil and water conservation factor. We used the national classification of erosion risk (SL190-2007) to categorize A, the average soil loss per

unit area by erosion, into six classes of erosion (Table S2).

(1) *R* factor

The *R* factor was calculate by the method modified by Arnoldus (1980) based on Wischmeier and Smith (1978) method as follows:

$$\mathrm{R} = \sum_{i=1}^{12} \left(1.735 \times 10^{1.5 \times log\frac{pi^2}{p} - 0.8188} \right)$$

where *p* and *pi* represent the annual average and monthly average rainfall, and *i* represents the month.

The rainfall data were obtained from the 4 meteorological stations closest to the study area in 2014 and 2017, and then we used the Kriging spatial interpolation in ArcGIS to generate the spatially distributed map for the *R* factor (Fig. S1).

(2) *K* factor

The *K* factor is a function of soil texture and structure (Thomas et al., 2018). In this study, the *K* factor was measured with the EPIC method (Williams, 1990) (Fig. S2), as follows:

$$\mathrm{K} = \left\{ 0.2 + 0.3exp\left[-0.0256SAN\left(1 - \frac{SIL}{100} \right) \right] \right\} \cdot \left(\frac{SIL}{CLA + SIL} \right)^{0.3} \cdot \left[1.0 - \frac{0.25SOC}{SOC + exp(372 - 295SPC)} \right] \cdot \left[1.0 - \frac{0.7SN_1}{SN_1 + exp(-5.51 + 22.9SN_1)} \right]$$

where *CLA*, *SAN* and *SIL*, are the mass fractions (%) of clay, sand and silt, ($SAN1 = 1 - SAN/100$), *SOC* is the mass fraction of soil organic carbon (%)

(3) *LS* factor

The *L* and *S* factors are the main topographic attributes that influence soil erosion

(Datta & Schack-Kirchner, 2010). In this study, L and S were calculated using the following expressions (McCool et al., 1987; McCool et al., 1989; Zhang et al., 2013):

$$L = \left(\frac{\lambda}{22.13}\right)^{\alpha}$$

$$\alpha = \left(\frac{\beta}{\beta + 1}\right)$$

$$\beta = \frac{\sin\theta}{3 \times (\sin\theta)^{0.8} + 0.56}$$

$$\begin{cases} S = 10.8 \times sin\theta + 0.03 (\theta < 9\%) \\ S = 16.8 \times sin\theta - 0.05 (\theta \geq 9\%) \end{cases}$$

where λ is the length of slope, θ is the slope, α is the variable length-slope exponent, and β is a factor that varies with the slope gradient (Fig. S3).

(4) *C* and *P* factors

The *C* and *P* factors showed very strong spatial heterogeneity in different regions (Xu and Shao, 2006). Vegetation is known to reduce soil erosion to a certain extent. A high value of the vegetation coverage factor *C*, shows weak resistance to soil erosion. The soil and water conservation factor *P* is the ratio of soil loss after taking soil conservation measures to the soil loss without taking soil conservation measures (Wischmeier and Smith, 1978). The *C* and *P* values were determined from previous studies (Feng et al., 2016), the land use status, and local farmland management surveys, and the *C* and *P* factor values were assigned to the corresponding land use types (Table 1) (Fig. S4; Fig. S5).

2.3 Soil erosion caused by the well pad and pipeline

The boundaries of the 42 well pads and 39 pipelines (15 well pads and 7 pipelines in 2014; 27 well pads and 32 pipelines in 2017) were identified using buffer

analysis in ArcGIS, to evaluate the influences of the shale gas development on soil erosion. The buffers around the well pads and pipelines were divided into 5 distances, 0–30, 30–60, 60–90, 90–120, and 120–150 m, respectively. We also selected areas with similar geographical conditions at least 1 km from the well pads and pipelines as controls. We had 5 well pad controls and 5 pipeline controls in 2014 and 7 well pad controls and 6 pipeline controls in 2017, with an area range of 1-1.5hm^2.

The 'Analysis Tools-Identify' option in ArcGIS was applied to identify soil erosion areas, and to evaluate the soil erosion changes around the well pads, pipelines, and the controls in 2014 and 2017. We compared the soil erosion among distances from the well pads, pipelines, and controls, and identified the ranges of the influence of the completed well pad and pipeline on soil erosion with ArcGIS.

2.4 Geodetector

Geodetector was applied to identify the driving force behind elements by detecting their spatial layered heterogeneity (Zhou et al., 2018; Wang et al., 2010).

(1) Factor detection

We use the factor detection to detect the spatial heterogeneity of soil erosion and identify the key driver factors behind the variation in soil erosion on the site around the well pads. This is represented by q, and the values of the detection force can be expressed as follows:

$$q = 1 - \frac{\sum_{h=1}^{L} N_h \sigma_h^2}{N\sigma^2} = 1 - \frac{SSW}{SST},$$

$$SSW = \sum_{h=1}^{L} N_h \sigma_h^2, SST = N\sigma^2,$$

where h is 1, 2, 3, etc.; L is the layer of the variable Y or factor X; N and N_h are the

sample sizes in the study area and layer; h, σ^2, and σ^2_h are the Y-value variances of the whole region and layer h, and SSW and SST are the variance of the intra-layer and the whole region, respectively. The q value is the explanatory force of factor X on the change in soil erosion. The value range of q is [0,1].

(2) Interaction detection

We used the interaction detection to identify the interactions between evaluation factors, i.e., whether the combined effects of the evaluation indicators X1 and X2 would increase or decrease the explanatory power of soil erosion, or whether the effects of these evaluation indicators on soil erosion are independent of each other. The q values of soil erosion were calculated first. The q value of the interaction of the two indexes was calculated, and the sum of the q values, q (X1∩X2) and q were compared. Based on the relationship between the three, the interactions were divided into five categories (Table S3)

The main influences on soil erosion within the sphere of influence of the pad were determined as the distance from the site to the pad (X1), pad area (X2), land use (X3), slope (X4), aspect (X5), elevation (X6), and NDVI (X7). The data of land use were classified by category, and the other indicators were grouped with the data processing method (Cao et al., 2013) (Table S4).

3. Results

3.1 Soil erosion in the shale gas development zone

In the study area, the ranges and the average values of the soil erosion rates in 2014 and 2017 were 0–243.41 and 0–323.31 t ha^{-1} a^{-1}, and 18.10 and 25.72 t ha^{-1} a^{-1},

respectively. The soil erosion intensities were mainly classified as micro and mild. About 107.65 t, or 0.02% of the total soil erosion, in 2014 was directly attributable to the completed well pads and pipelines, while about 924.45 t, or 0.12 %, of the total erosion, in 2017 was directly attributable to the completed well pads and pipelines (Fig. 2).

In 2014 and 2017, micro erosion accounted for 55% and 49% of the erosion from the well pads controls, respectively. In 2014, the proportions of erosion from the well pad buffer zones at 90–120 m and 120–150 m were similar to those of the controls. The proportions of micro erosion were higher for the pad, 0–30 m, 30–60 m, and 60–90 m than for the control. The erosion on the well-pad was classified as micro, and the well pad influenced the surrounding soil erosion to a distance of 90 m (Fig. 3a). In 2017, the proportion of micro erosion in the well pad buffer zone was higher at the pad, 0–30 m, and 30–60 m than for the control, and the well pad influenced the soil erosion to a distance of 60 m (Fig. 3b).

Micro erosion accounted for 46% and 37% of the erosion from the pipeline controls in 2014 and 2017, respectively. The micro and mild erosion for the entire pipeline buffer zone (0–150 m) and the control were similar and differed by only 1%–4% (Fig. 3c, Fig. 3d). The proportion of erosion that was classified moderate and above over the pipelines was greater than for the control and reached 32% and 55% in 2014 and 2017, respectively. The soil erosion caused by the completed pipelines was mainly concentrated directly over the pipelines.

The soil erosion intensity in the immediate pipeline area, which was higher in 2017

than that in 2014 was higher than the intensities at the different distances in the buffer zone. This difference between 2017 and 2014 mainly reflects the slope gradient. In 2014, the pipelines were mainly distributed in areas with slopes ranging from 18.1°–30.2°, while 15.7 km of the pipelines were on steep slopes ranging from 20.5°–32.5° in 2017.

3.2 Factors influencing changes in soil erosion in the shale gas pad buffer zones

The results from factor detection showed that the soil erosion at different distances from the well pad in 2014 and 2017 was mainly affected by land use and slope, and land use and slope explained less of the soil erosion in 2017 than in 2014 (Fig. 4). We compared the impact of land use and slope on soil erosion around the completed shale gas well pads in 2014 and 2017. In 2014, the land use in the well pad buffer zones comprised, on average, 2.23 ha of dry land, 1.88 ha of paddy field, 1.55 ha of forest, and 0.94 ha of shrub land. In 2017, the land use in the well pad buffer zones comprised, on average, 1.50 ha of dry land, 1.15 ha of paddy field, 2.06 ha of forest, and 1.87 ha of shrub land (Fig. 5a). The average slopes of the well pad buffer zones were 12.0° and 16.0° in 2014 and 2017, respectively (Fig. 5b),

The results from interaction detection analysis showed that the interactions of land use ∩ slope in the well pad buffer zone were 0.573 and 0.217 in 2014 and 2017, respectively, and were the most significant influences on soil erosion. The interactions of land use ∩ elevation were ranked next, with values of 0.464 and 0.186 in 2014 and 2017, respectively (Fig. 6).

4. Discussion

The shale gas well pad influenced soil erosion in 2014 and 2017 to distances of 90 and 60 m, respectively. This is similar to the extent of the influence of the well pad on the NPP in the same shale gas development zone observed by Guo et al. (2020). Erosion was inhibited to up to 30 m from the completed well pad, mainly reflecting the hardening of soil (Fink et al., 2014; Livy et al., 2018). The reduction in soil erosion in the 30–60 m buffer zone reflects the construction of access roads and auxiliary facilities to support the shale gas development (Kiviat, 2013; Milt et al., 2016; Racicot et al., 2016), while the lower intensity of soil erosion in the 60–90 m buffer zone reflects the construction of temporary accommodation and roads. Because of improvements in mining technology between 2014 and 2017, personnel were no longer needed at the well pads, meaning that there was no need to construct temporary accommodation in the 60–90 m buffer. The soil erosion intensity in the 60–90 m buffer zone in 2017 was similar to that in the controls because the well pads were closer to the original road.

Land use was a major influence on the soil erosion around the well pads. Unlike similar shale gas development areas in the US, where soil is left exposed (Pierre et al., 2015; Castro et al., 2017), the permanent and semi-permanent infrastructure (such as foundations and flowback pool) around the well pads in this area was secured with cement, asphalt, and other stabilizers, which may have reduced the water erosion. Before 2014, to reduce transportation and labor costs, well pads were mainly distributed in areas with frequent human activities, so the cultivated land round the

well pads changed to construction. A series of environmental protection laws and oil and gas industrial regulations were issued and implemented in 2015, meaning that new well pads had to be located far from areas with frequent human activities (NPC, 2015). The land use around the well pads in this area mainly changed from forest and shrub to construction land. The C values of dry land (0.22) and paddy field (0.1) were greater than those for forest (0.006) and shrub (0.01), which shows that land use explained more soil erosion in 2014 than in 2017.

Slope also influenced the changes in soil erosion around the well pads. In 2014 and 2017, the average slopes in the well pad area were 12° and 16°, respectively. While the well pads in shale gas development zones in the US were mainly arranged in gently sloping areas (Meng, 2014), they were on steeper slopes in this study area, with high risks of soil erosion. From their study in a karst area, Xiong et al. (2012) reported that the amount of soil erosion from the same land use type was significantly and positively correlated with the slope when the slope < 15°, but the amount of soil erosion only increased slowly and even decreased slightly in some areas when the slope ≥ 15°; this helps to explain why the explanatory power of slope on soil erosion was only slightly higher in 2017 than in 2014.

The interaction between land use and slope was the strongest, followed by the interaction between land use and elevation, which means that the hard soil around the shale gas well pad in the area with the steep slope and at a high altitude had a strong inhibitory effect on soil erosion. Xu and Shao (2006) reported that the risk of soil erosion in karst areas was highest on dry land with a slope of between 6°–20°. In 2014,

well pads were mainly located on steeply sloping dry land, which also explains why the interaction intensity was much higher in 2014 than in 2017. In this study area, there was strong spatial heterogeneity between elevation and land use in 2014. In 2014, the well pad areas at low altitude were mainly on residential land, while those at high altitude were mainly on dry land. However, in 2017, the well pads were mainly on forest and shrub land (Guo et al., 2020), and the elevation and land use were largely homogeneous. The interactions between land use and elevation were therefore stronger in 2014 than in 2017.

In the study area, 15.7 km of pipelines were laid on steep slopes, and the forest was not restored over the pipeline. The land was mainly grassed or left bare (Guo et al., 2021), with the latter susceptible to soil erosion. Drohan and Brittingham (2012) reported that the pipeline laying was the main influence on soil erosion through the shale gas development process, and that much more soil was eroded from the damaged surface area than from the well pads and roads (Souther et al., 2014; Adams et al., 2011). Qi et al. (2012) studied soil erosion around natural gas pipelines and found that, as in this study, there was less soil erosion from the land on either side of the completed pipelines. After the pipelines were laid in the Eagle Ford Shale Gas Development Zone in the US, the vegetation cover over the pipelines was restored, so relatively little soil was eroded from over the pipelines (Pierre et al., 2015). Elsewhere, roads built around shale gas development zones were a major influence on soil erosion (Mcbroom et al., 2012). Few roads were developed specifically for the shale gas development activities. Any roads constructed were generally within a distance of

120–140 m (Guo et al., 2021) and so were incorporated into the well pad buffer zone.

In this study, we calculated the *LS* factor with the improved method of Zhang et al. (2013). This method has been applied numerous times in karst areas with good results (Gao and Wang, 2019; Wang, 2001). Hu et al. (2015) found that the *LS* factors obtained from the RUSLE and USLE models were not significantly different. However, the results obtained when the two models were applied to karst areas were quite different, because of the steep slopes and geomorphic differences (Liu et al., 2013; Dai et al., 2017). In future studies, the *LS* factor should be calculated for different landforms and soil types. The *C* and *P* factors are derived from the land type assignment, so their accuracy is mainly determined by the accuracy of the land use type interpretation. The 2014 and 2017 land use classifications used in this study were obtained by interpreting remote sensing images with resolutions of 2.1×2.1 m and 1.5×1.5 m, which were 94.2% and 98.2% accurate, respectively (Guo et al., 2020; Guo et al., 2021), and so met the accuracy requirements of the RUSLE model. Furthermore, the accuracy of the *K* factor could be improved by analyzing the texture of soil samples from the area.

5. Conclusions

In this study, the RUSLE model and Geodetector were used to explore the impact of the completed well pads and pipelines on soil erosion in a shale gas development zone. The results showed that the shale gas development accounted for about 0.02% and 0.12% of the total erosion in 2014 and 2017, respectively. The impacts of the

completed well pads on soil erosion extended to 90 and 60 m around the well pads in 2014 and 2017, respectively. Soil erosion related to the completed pipelines was mainly limited to the soil covering the pipeline and had little impact on the surrounding area. The soil erosion intensity at different distances around the completed well pads was mainly affected by the land use and slope, and the explanatory power was weaker in 2017 than in 2014. The completed pipelines were the main influence on soil erosion. We suggest that the pipelines should be arranged in gently sloping areas if the economic and technical conditions permit. Studies should explore how to restore the vegetation over the pipelines so that soil erosion can be decreased.

Acknowledgments

This study was jointly financed by the National Science and Technology Major Project (2016ZX05040-002) and the China National Petroleum and Natural Gas Corporation Major Scientific and Technological Project (2016E-1205).

References

Adams, M. B., Edwards, P. J., Ford, W.M., Johnson, J.B., Schuler, T.M., Gundy, T.V., Wood, F., 2011. Effects of development of a natural gas well and associated pipeline on the natural and scientific resources of the Fernow Experimental Forest. Newtown Square, PA: U.S. Department of Agriculture, Forest Service, Northern Research Station, 1-24. https://www.fs.fed.us/nrs/pubs/gtr/gtr_nrs76.pdf

Arnoldus, H.M.J., 1980. An approximation of the rainfall factor in the Universal Soil

Loss Equation. In: De Boodt, M., Gabriels, D., Eds., Assessment of erosion. FAO Land and Water Development Division, Chichester UK: Wiley, 127–132.

Cao, F., Ge, Y., Wang, J. F., 2013. Optimal discretization for geographical detectors-based risk assessment. Gisci. Remote Sens. 50(1), 78–92.

Castro. A. F., Marsters, P., Diego, P., Kammen, D. M., 2017. Sustainability lessons from shale development in the United States for Mexico and other emerging unconventional oil and gas developers. Renew. Sust. Energ. Rev. 82(1), 1320–1332.

Chen, H., Takashi, O., Wu, Pan., 2017. Assessment for soil loss by using a scheme of alterative sub-models based on the RUSLE in a Karst Basin of Southwest China. J. Integr. Agr. 16(2), 377–388. (in Chinese)

Chen, H.K., Du, X.Y., Guo, Y., Zhang, X.Y., Wu, Q., Wang, Q.B., He, J.A., Ma,L., 2018. Influences of shale gas well-pad development on land use and vegetation biomass in a shale gas mining area. Chin. J. Appl. Ecol. 29(10), 3377–3384. (in Chinese)

Chinas National Peoples Congress., 2015. Environmental Protection Law of the People's Republic of China. https://www.mee.gov.cn/ywgz/fgbz/fl/201404/t20140425_271040.shtml

Dai, Q.H., Peng, X.D. Yang. Z., Zhao. L.S., 2017. Runoff and erosion processes on bare slopes in the karst rocky desertification area. Catena 152, 218–226.

Datta, P. S., Schack, K. H., 2010. Erosion Relevant Topographical Parameters Derived from Different DEMs—A Comparative Study from the Indian Lesser Himalayas. Remote Sens. 2(8), 1941–1961.

Donnelly, S., 2018. Factors influencing the location of gathering pipelines in Utica and Marcellus shale gas development. Journal of Geography and Earth Sciences 6(1), 1–10.

Drohan, P. J., Brittingham, M., 2012. Topographic and soil constraints to shale-gas development in the Northcentral Appalachians. Soil Sci. Soc. Am. J. 76(5), 1696–1706.

Feng, T., Chen, H.S., Polyakov, V.O., 2016. Soil erosion rates in two karst peak-cluster depression basins of northwest Guangxi, China: Comparison of the RUSLE model with ^{137}Cs measurements. Geomorphology 253: 217–224.

Fink, C.M., Drohan, P.J., 2014. Dynamic soil property change in response to reclamation following northern Appalachian natural gas infrastructure development. Soil Sci. Soc. Am. J. 79, 147–154.

Gao, J.B., Wang, H., Zuo, L.Y., 2018. Spatial gradient and quantitative attribution of karst soil erosion in Southwest China. Environ. Monit. Assess.190(730), 2–13.

Guo, Y., Du, X.Y., Chen, H.K., Zhang, X.Y., Wang, Q.B. 2021, Influence of shale gas development on core forest in a subtropical karst region in China. Sci. Total Environ. 771, 145287.

Guo, Y., Zhang, X.Y., Wang, Q.B., Chen, H.K., Du, X.Y., Ma, Y.P., 2020.Temporal changes in vegetation around a shale gas development area in a subtropical karst

region in southwestern China. Sci. Total Environ. 701, 134769.

Hu, G., Song, H., Liu, B. Y., Shi, X. J., Zhang, X. L., Fang, H. Y., 2015. Effects of both slope length of standard plot and algorithms of LS on calculated values of topography factor (LS) in black soil areas in Northeast China. Trans. Chin. Soc. Agric. Eng. 31(03):166–173. (in Chinese)

Jin, F. M., Yang, W. C., Fu, J. X., Li, Z., 2021. Effects of vegetation and climate on the changes of soil erosion in the Loess Plateau of China. Sci. Total Environ. 773, 145514.

Johnson, N. 2010. Pennsylvania energy impacts assessment. The Nature Conservancy, Harrisburg, PA. http://www.nature.org/media/pa/tnc_energy_analysis.pdf

Kiviat, E., 2013. Risks to biodiversity from hydraulic fracturing for natural gas in the Marcellus and Utica shales. Ann. NY Acad.Sci. 1286, 1–14.

Liu, Z.T., Ni, J.P., Yang, Z., 2013.Bare slope erosion experimental research under the condition of artificial rainfall precipitation in Karst area. J. Soil Water Conserv. 27(5), 12–16. (in Chinese)

Livy, M.R., Gopalakrishnan, S., Klaiber, H.A., Roe, B. E., 2018. The impact of intensity on perceived risk from unconventional shale gas development. J. Environ. Manage. 218, 630–638.

Ma, Q.H., Zhang, K. l., 2018. Progresses and prospects of the research on soil erosion in Karst area of Southwest China. Advances in Earth Science 33(11), 1130–1141. (in Chinese)

Mcbroom, M., Thomas, T., Zhang Y., 2012.Soil erosion and surface water quality

impacts of natural gas development in East Texas, USA. Water 4(4), 944–958.

McCool, D. K., Brown, L. C., Foster, G. R., Mutchler, C. K., Meyer, L. D., 1987. Revised slope steepness factor for the universal soil loss equation. Transactions of the Asae 30(5), 1387–1396.

McCool, D. K., Foster, G. R., Mutchler, C. K., Meyer, L. D., 1989. Revised slope length factor for the universal soil loss equation. Transactions of the Asae, 32(5), 1571–1576.

Meng, Q.M., 2014. Modeling and prediction of natural gas fracking pad landscapes in the Marcellus Shale region, USA. Landsc. Urban Plan 121, 109–116.

Milt, A.W., Gagnolet, T., Armsworth, P.R., 2016.Synergies and tradeoffs among environmental impacts under conservation planning of shale gas surface infrastructure. Environ. Manage. 57(1), 21–30.

Ministry of Water Resources of PR China, 2007. Standard for Classification and Gradation of Soil Erosion SL 190–2007. China Waterpower Press, Beijing, China.

National Meteorological Information Center, 2017, Climate Data Online, Precipitation and Temperature Data. http://data.cma.cn/dataService/cdcindex/datacode/A.0029.0005/show_value/normal.html.

Pierre, J. P., Abolt, C, j., Young, M. H., 2015. Impacts from above-ground activities in the eagle ford shale play on landscapes and hydrologic flows, La Salle County, Texas. Environ. Manage. 55(6), 1262–1275.

Qi, S. S., Hao, F. H., Ouyang, W., Cheng, H. G., 2012. Characterizing landscape and soil erosion dynamics under pipeline interventions in southwest China. Procedia Environmental Sciences, 13, 1863–1871.

Racicot, A., Babin-Roussel, V., Dauphinais J F., Joly, J.S., Noël, P., Lavoie, C., 2014. A framework to predict the impacts of shale gas infrastructures on the forest fragmentation of an agroforest region. Environ. Manage. 53(5), 1023–1033.

Renard, K.G., Foster, G.R., Weesies, G.A., McCool, D.K., Yoder, D.C., 1997. Predicting soil erosion by water: a guide to conservation planning with the Revised Universal Soil Loss Equation (RUSLE). USDA Agriculture Research Service Handbook 703, USA: 1–384.

Souther, S., Tingley, M. W., Popescu, V. D., Hayman, D. T., Ryan, M. E., Graves, T. A., 2014. Biotic impacts of energy development from shale: research priorities and knowledge gaps. Front. Ecol. Environ. 12 (6), 330–338.

Thomas, J., Joseph, S., Thrivikramji, K.P., 2018. Assessment of soil erosion in a tropical mountain river basin of the southern Western Ghats, India using RUSLE and GIS. Geosci. Front. 9(3), 281–294.

Wachal, D. J., Banks, K. E., Hudak, P. F., Harmel, R. D., 2009. Modeling erosion and sediment control practices with RUSLE 2.0: a management approach for natural gas well sites in Denton County, TX, USA. Environ. Geol. 56(8), 1615–1627.

Wang, W. F., 2001. Investigation of land erosion model of Houzhaihe catchment in Puding, Guizhou and its application. Guizhou Geology 18(2), 99–106. (in Chinese)

Wang, F., Liu, R., Yang, Q. K., 2003. A study on soil erosion and soil and water conservation of highway construction. Highway 2003(S1), 148–152. (in Chinese)

Wang, H., Gao, J.B., Hou, W.J., 2018. Quantitative attribution analysis of soil erosion in different morphological types of geomorphology in karst areas: Based on the geographical detector method. Acta Geographica Sinica 73(9), 1674–1686. (in Chinese)

Wang, J.F., Li, X.H., Christakos, G., Liao, Y.L., Zhang, T., Gu, X., Zheng, X.Y., 2010. Geographical detectors-based health risk assessment and its application in the neural tube defects study of the heshun region, China. Int. J. Geogr. Inf. Sci. 24(1), 107–127.

Wang, J.F., Xu, C.D., 2017. Geodetector: principle and prospective. Acta Geographica Sinica 72(1), 116–134. (in Chinese)

Wang, J.L., Liu, M.M., Bentley, Y.M., 2018.Water use for shale gas extraction in the Sichuan Basin, China. J. Environ. Manage. 226, 13–21.

Williams, J. R., 1990.The erosion-productivity impact calculator (EPIC) model: a case history. Philos T Roy Soc B. 329(1255), 421–428.

Wischmeier, W.H., Smith, D.D., 1978. Predicting rainfall erosion losses: a guide to conservation planning. USDA Washington, D. C. 537, 1–58.

Xiong, K. N., Li, J., Long, M. Z., 2012. Features of soil and water loss and key issues in demonstration areas for combating Karst rocky desertification. Acta Geographica Sinica 67(7), 878–888. (in Chinese)

Xu, Y. Q., Shao, X. M., 2006. Estimation of soil erosion supported by GIS and RUSLE: A case study of Maotiaohe watershed, Guizhou Province. Journal of Beijing Forestry University 28(4), 67–71. (in Chinese)

Yang, D., Kanae, S., Oki, T., Koike, T., Musiake, K., 2003. Global potential soil erosion with reference to land use and climate changes. Hydrol. Processes 17(14), 2913–2928.

Zeng, C., Wang, S.J., Bai, X.Y., Li, Y.B., Tian, Y.C., Li, Y., Wu, L.H., Luo, G.J., 2017. Soil erosion evolution and spatial correlation analysis in a typical karst geomorphology using RUSLE with GIS. Solid Earth Discuss 8(4), 721–736.

Zhang, H.M., Yang, Q.K., Li, R., Liu, Q.R., Moore, D., He, P., Ritsema, C. J., Geissen, V., 2013. Extension of a GIS procedure for calculating the RUSLE equation LS factor. Comput. Geosci. 52, 177–188.

Zhou, T., Jiang, G. H., Zhang, R. J., Zheng, Q. Y., Ma, W. Q., Zhao, Q. L., Li, Y.L., 2018. Addressing the rural in situ urbanization (RISU) in the Beijing–Tianjin–Hebei region: Spatio-temporal pattern and driving mechanism. Cities 75, 59–71.

Zou, C.N., Dong, D.Z., Wang, Y.M., Li, X.J., Huang, J.L., Wang, S.F., Guan, Q.Z., Zhang, C.C., Wang, H.Y., Liu, H.L., Bai, W.H., Liang, F., Lin, W., Zhao, Q., Liu, D.X., Yang, Z., Liang, P.P., Sun, S.S., Qiu, Z., 2015. Shale gas in China: characteristics, challenges and prospects (I). Pet. Explor. Dev. 42 (6), 753–767.

Credit author statement

Yu Guo: Formal analysis, Data curation, Visualization, Writing- Original draft preparation.

Xianyuan Du: Conceptualization, Writing- Original draft preparation.

Dandan Li: Investigation, Writing- Original draft preparation.

Guodi Zheng: Supervision, Writing- Original draft preparation & Editing.

Xinyu Zhang: Supervision, Writing - Review & Editing.

Hongkun Chen: Methodology, Supervision, Writing - Review & Editing.

Jin Zheng: Software, Writing - Review & Editing

Declaration of interests

☑The authors declare that they have no known competing financial interests or personal relationships that could have appeared to influence the work reported in this paper.

☐The authors declare the following financial interests/personal relationships which may be considered as potential competing interests:

Figure captions

Fig. 1 A: The location of shale gas development zone in Sichuan Province, South West China. B: The distribution of completed shale gas well pads and pipelines, C: A well pad field, D: A pipeline field.

Fig. 2 Spatial distribution of the soil erosion intensity in 2014 and 2017.

Fig. 3 The soil erosion intensities of the shale gas well pads, pipelines, and their buffer zones and controls in 2014 and 2017.

Fig. 4 The *q* values of the factors impacting soil erosion on the 0–90 m buffer zone of the well pads in 2014 and the 0–60 m buffer zone of the well pads in 2017. Note: ** ($p < 0.01$), and * ($p < 0.05$) denote that the *q* value is significant in the buffer zone.

Fig. 5 The main influences on the 0–90 m buffer zone of the well pads in 2014 and the 0–60 m buffer zone of the well pads in 2017.

Fig. 6 The interaction between pairs of factors impacting soil erosion in the 0–90 m buffer zone of the well pads in 2014 and the 0–60 m buffer zone of the well pads in 2017 Note: Distance from the sites to the pads (X1), Pad area (X2), Land use (X3), Slope (X4), Aspect (X5), Elevation (X6), and NDVI (X7).

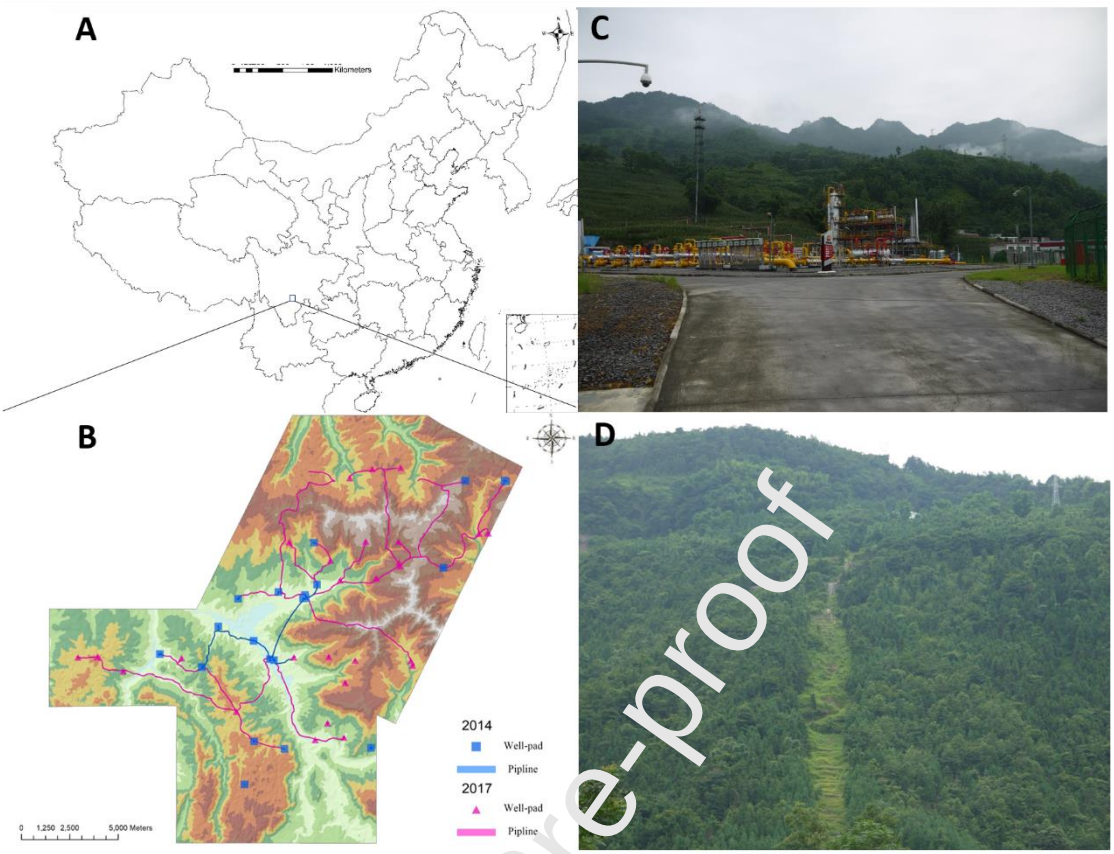

Fig. 1 A: The location of shale gas development zone in Sichuan Province, South West China. B: The distribution of completed shale gas well pads and pipelines, C: A well pad field, D: A pipeline field.

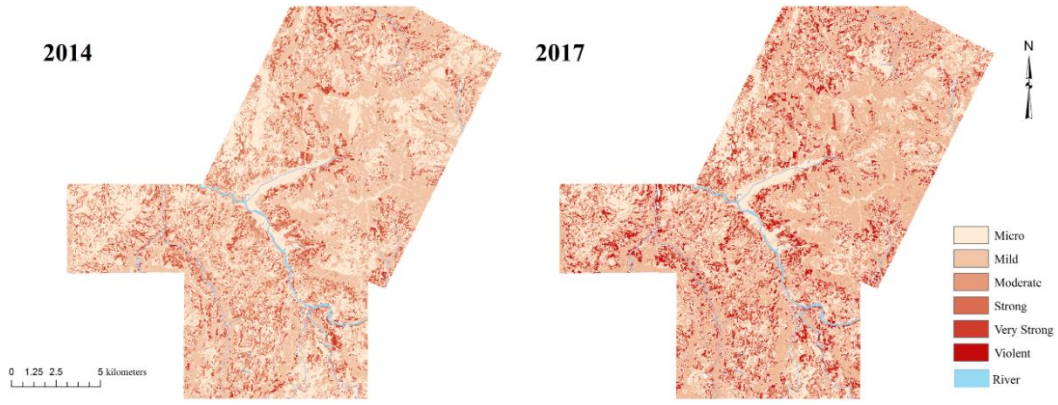

Fig. 2 Spatial distribution of the soil erosion intensity in 2014 and 2017.

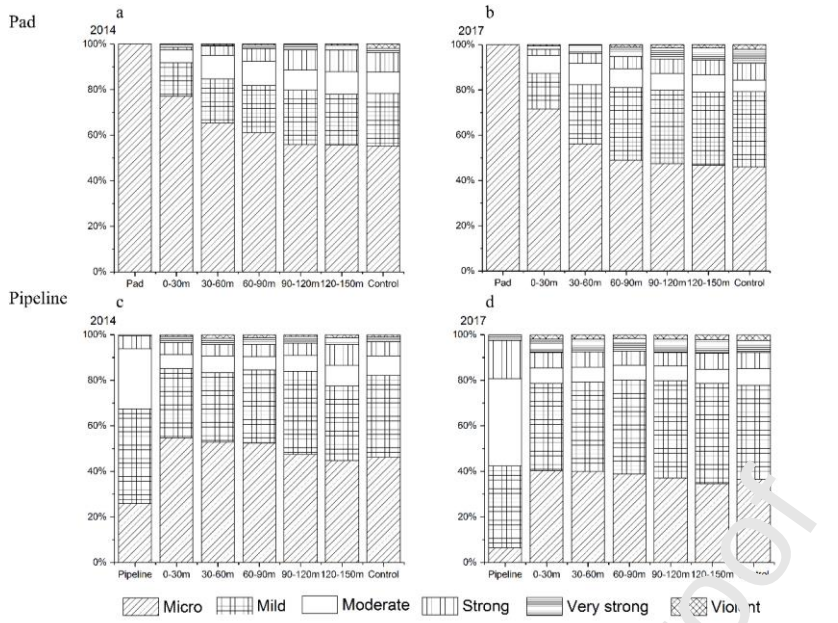

Fig. 3 The soil erosion intensities of the shale gas well pads, pipelines, and their buffer zones and controls in 2014 and 2017.

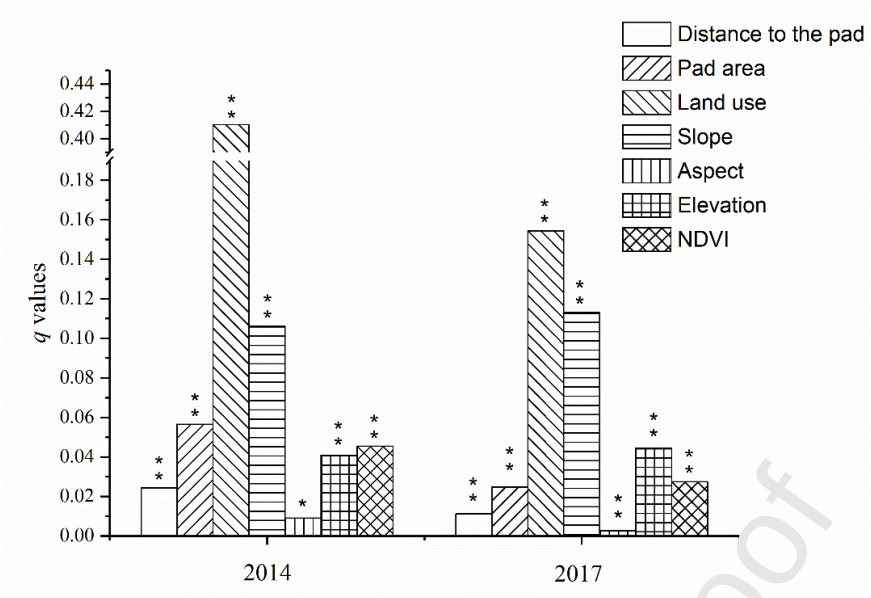

Fig. 4 The *q* values of the factors impacting soil erosion on the 0–90 m buffer zone of the well pads in 2014 and the 0–60 m buffer zone of the well pads in 2017. Note: ** ($p < 0.01$), and * ($p < 0.05$) denote that the *q* value is significant in the buffer zone.

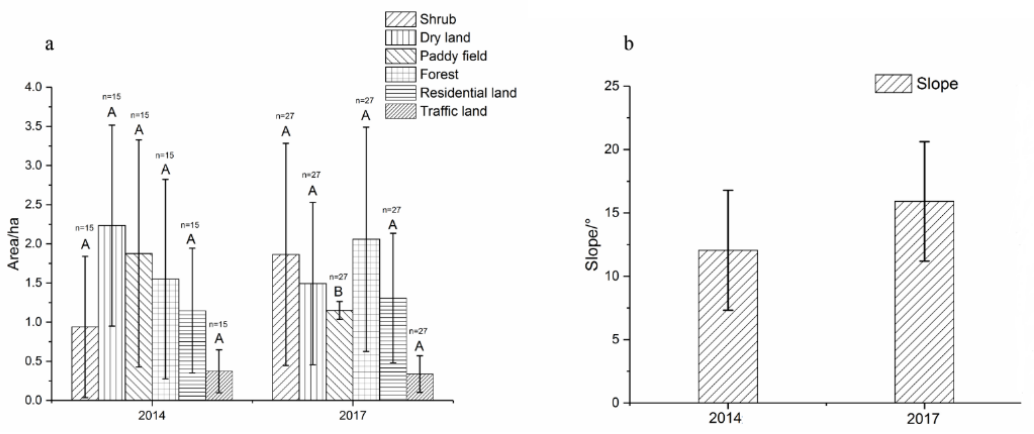

Fig. 5 The main influences on the 0–90 m buffer zone of the well pads in 2014 and the 0–60 m buffer zone of the well pads in 2017.

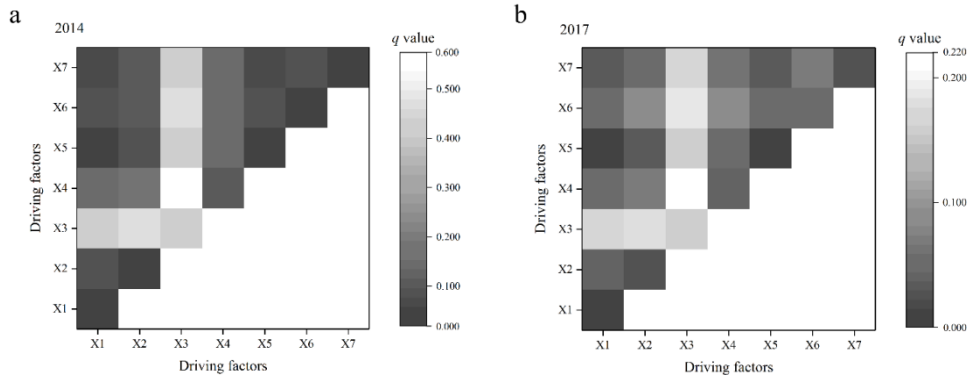

Fig. **6** The interaction between pairs of factors impacting soil erosion in the 0–90 m buffer zone of the well pads in 2014 and the 0–60 m buffer zone of the well pads in 2017 Note: Distance from the sites to the pads (X1), Pad area (X2), Land use (X3), Slope (X4), Aspect (X5), Elevation (X6), and NDVI (X7).

Table 1 *C* values and *P* values

Land use	Paddy field	Dry land	Forest	Orchard	Shrub	Grass land	Water	Residential land	Traffic land	Mining land	Bare land
C value	0.10	0.22	0.006	0.01	0.01	0.04	0	0	0	0	0
P value	0.15	0.40	1.0	1.0	1.0	1.0	0	0	0	0	0

Graphical abstract

The completed well-pad and its buffer zone

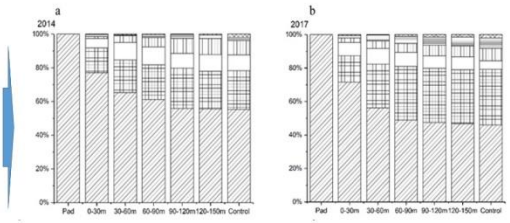

The soil erosion intensity of well-pads and their buffer zones and controls in 2014 and 2017

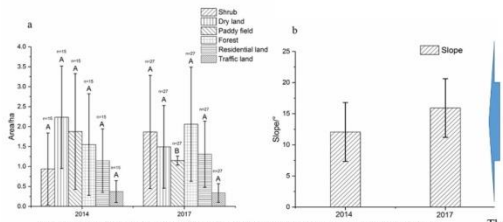

The main impact factors on the 0-90m buffer zone of the pads in 2014 and the 0-60m buffer zone of the pads in 2017.

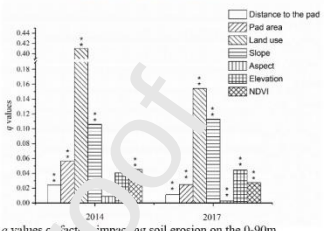

The q values of factors impacting soil erosion on the 0-90m buffer zone of the well-pads in 2014 and the 0-60m buffer zone of the well-pads in 2017. Note: **, and * denote that q value is significant at level of 0.01 ($p < 0.01$), 0.05 ($p < 0.05$).

Highlights

- The influences on soil erosion around the well pads were evaluated by Geodetector.
- The pipelines caused more soil erosion than the well pads.
- Well pads erosion affected up to 90 and 60 m in 2014 and 2017, respectively.
- Soil erosion intensity around the well pads was related to the land use and slope.
- Pipeline-related erosion were 32% and 55% of total in 2014 and 2017, respectively.